



Original Article

Validation of Serpent-SUBCHANFLOW-TRANSURANUS pin-by-pin burnup calculations using experimental data from the Temelín II VVER-1000 reactor



Manuel García ^{a,*}, Radim Vočka ^b, Riku Tuominen ^c, Andre Gommlich ^d, Jaakko Leppänen ^c, Ville Valtavirta ^c, Uwe Imke ^a, Diego Ferraro ^a, Paul Van Uffelen ^e, Lukáš Milisdörfer ^f, Victor Sanchez-Espinoza ^a

^a Karlsruhe Institute of Technology, Institute of Neutron Physics and Reactor Technology, Hermann-von-Helmholtz-Platz 1, 76344, Eggenstein-Leopoldshafen, Germany

^b ÚJV Rež a. s., Hlavní 130, Rež, Czech Republic

^c VTT Technical Research Centre of Finland Ltd., P.O. Box 1000, FI-02044, VTT, Finland

^d Helmholtz-Zentrum Dresden-Rossendorf, Institute of Resource Ecology, Bautzner Landstraße 400, 01328, Dresden, Germany

^e Joint Research Centre, European Commission, Hermann-von-Helmholtz-Platz 1, 76344, Eggenstein-Leopoldshafen, Germany

^f ČEZ a. s., Duhová 2 / 1444, Prague, Czech Republic

ARTICLE INFO

Article history:

Received 12 January 2021
Received in revised form
5 April 2021
Accepted 22 April 2021
Available online 8 May 2021

Keywords:

Monte Carlo neutron transport
Subchannel thermalhydraulics
Fuel-performance analysis
High-fidelity multiphysics
Pin-level burnup
VVER-1000

ABSTRACT

This work deals with the validation of a high-fidelity multiphysics system coupling the Serpent 2 Monte Carlo neutron transport code with SUBCHANFLOW, a subchannel thermalhydraulics code, and TRANSURANUS, a fuel-performance analysis code. The results for a full-core pin-by-pin burnup calculation for the ninth operating cycle of the Temelín II VVER-1000 plant, which starts from a fresh core, are presented and assessed using experimental data. A good agreement is found comparing the critical boron concentration and a set of pin-level neutron flux profiles against measurements. In addition, the calculated axial and radial power distributions match closely the values reported by the core monitoring system. To demonstrate the modeling capabilities of the three-code coupling, pin-level neutronic, thermalhydraulic and thermomechanic results are shown as well. These studies are encompassed in the final phase of the EU Horizon 2020 McSAFE project, during which the Serpent-SUBCHANFLOW-TRANSURANUS system was developed.

© 2021 Korean Nuclear Society, Published by Elsevier Korea LLC. This is an open access article under the CC BY-NC-ND license (<http://creativecommons.org/licenses/by-nc-nd/4.0/>).

1. Introduction

Within the EU Horizon 2020 McSAFE project [1], a simulation tool based on Serpent 2 [2], SUBCHANFLOW (SCF) [3] and TRANSURANUS (TU) [4] was developed, coupling continuous-energy Monte Carlo neutron transport, subchannel thermalhydraulics and fuel-performance analysis [5]. This three-code coupling combines high-fidelity neutronics with pin-by-pin thermalhydraulic and thermomechanical analysis to achieve a high level of detail in depletion simulations. One of the main objectives of the project is to use this methodology to calculate burnup-dependent pin-level safety parameters at pin level for Light Water Reactor (LWR)

designs. To apply this tool to full-core burnup problems, for which the memory demand becomes massive, a Collision-based Domain Decomposition (CDD) scheme has been developed to provide memory scalability to Serpent 2 [6] and hence to the simulation system. As part of the final stage of McSAFE, this tool is being validated using pin-level experimental data from PWR and VVER reactors. In similar high-fidelity reactor physics projects, neutronic-thermalhydraulic coupled systems such as RMC/CTF [7], as well as neutronic-thermomechanical tools like MCS/FRAPCON [8], have been used to tackle full-core burnup problems such as the BEAVRS PWR benchmark.

The focus of this work is the validation of Serpent–SCF–TU pin-level burnup capabilities for the Temelín II VVER-1000 Nuclear Power Plant (NPP). For the ninth cycle of operation, which corresponds to a startup from a fresh core, the accuracy of the results is assessed using measured critical boron concentration and neutron

* Corresponding author.

E-mail address: manuel.garcia@kit.edu (M. Garcia).

flux profiles, as well as power distributions reported by the Core Monitoring System (CMS). Moreover, the advanced modeling capabilities of the three-code coupling are demonstrated with pin-level neutronic, thermalhydraulic and thermomechanic results.

The depletion calculation presented in this work serves to demonstrate the cutting-edge modeling capabilities developed as part of the McSAFE project. On the one hand, the burnup of the whole core is simulated at pin level using continuous-energy nuclear data and without major approximations in the geometrical model or the neutron transport calculation. This methodology provides a direct solution of the core state without relying on the traditional lattice- and core-level approaches typically used in the nuclear industry. On the other hand, the three-code coupling scheme ensures a consistent solution across physics and provides a highly detailed description of the core, in particular of the thermomechanical behavior of the fuel, which is generally only considered in a simplified manner in burnup calculations. Finally, the simulations shown here illustrate the use of High Performance Computing (HPC) systems to tackle these types of problems.

The depletion methodology used in Serpent–SCF–TU is presented in Section 2, where the CDD feature used to handle the memory footprint of the burnup calculation is briefly described as well. The Temelín II VVER-1000 NPP used as validation case, the operational data and the experimental measurements are presented in detail in Section 3. The modeling approach is discussed in Section 4, while the results are presented and analyzed in Section 5.

2. Serpent–SCF–TU burnup

The Serpent–SCF–TU coupling scheme is based on an object-oriented design with mesh-based feedback exchange, as detailed in Section 2.1. The depletion scheme, presented in Section 2.2, is semi-implicit, with fully coupled pin-by-pin feedback. The coupling methodology and its verification for pin-level fuel-assembly calculations has been described in full detail in previous publications [5,9]. To handle large-scale burnup calculations, burnable materials are distributed across computing nodes using the newly implemented CDD feature in Serpent 2 [6], as explained briefly in Section 2.3.

2.1. Coupling scheme

Fig. 1 shows the software design of the coupling system. The coupling interface for each code is implemented as a C++ solver class derived from a common base class, which masks the internal calculation methods, data structures and programming languages. Using the MEDCoupling open-source library [10], feedback fields are defined in unstructured meshes and code-to-code interpolations for data exchange are performed automatically at runtime. A C++ supervisor program implements the actual coupling scheme using object-oriented features. This methodology increases the maintainability and reusability of the code with respect to traditional approaches such as *master-slave* coupling, and therefore is particularly useful for this three-code coupling [5].

2.2. Depletion scheme

Fig. 2 shows the calculation and feedback scheme used for Serpent–SCF–TU coupled depletion for a step from time t_n to t_{n+1} . A semi-implicit algorithm is used, i.e. code-to-code feedback is done using the fields at the end of the step (EOS) and convergence at EOS is achieved iterating each burnup step. This improves the stability of the coupled solution relative to an explicit method and provides a converged state across physics for each burnup step.

For each iteration, a SCF steady-state calculation is performed

first to obtain the cooling conditions for the Serpent power distribution at EOS. Second, TU solves a burnup step from t_n to t_{n+1} using the SCF solution as boundary condition and the Serpent power as heat source, both at EOS. For the first iteration in each burnup step, when the Serpent solution at EOS has not yet been calculated, the power at the beginning of the step (BOS) is used in SCF and TU. Third, Serpent carries out a burnup iteration using the Stochastic Implicit Euler (SIE) method [11], with the thermalhydraulic conditions at EOS. The rationale for this code order is that (a) SCF calculates the boundary conditions for TU and receives no feedback from it and (b) the Serpent calculation is the most expensive step, and therefore should be performed with the latest thermalhydraulic data. It is important to note here that Serpent and TU perform independent burnup calculations, Serpent with the full set of Bateman equations [12] and TU with a reduced one suitable for fuel-performance analysis [13].

In this scheme, the pin power P calculated by Serpent is used in SCF as the heat source for the coolant and in TU considering a radial power distribution within the fuel pellet based on an empirical method included in the burnup model [13]. The coolant temperature T_{cool} and density ρ_{cool} calculated by SCF and the fuel temperature T_{fuel} obtained by TU are used in Serpent as thermalhydraulic feedback to the cross sections. For T_{fuel} either a radial average, an effective Doppler temperature or a radial profile can be used - the first option is used in this work. SCF provides the boundary conditions for TU (cladding-coolant heat-transfer coefficient $h_{clad-cool}$, T_{cool} and coolant pressure p). All the feedback is done at sub-channel- and pin-level.

As an alternative to this three-code coupling, the traditional neutronic-thermalhydraulic scheme can be used without TU. In this case, the fuel calculation is handled by SCF, which includes a simplified fuel-performance model based on fuel-cladding-gap evolution and irradiation-driven thermal-conductivity degradation. In Section 5 both approaches, i.e. with and without TU, are compared.

2.3. Domain decomposition scheme

The storage of burnable material compositions, nuclear data and reaction rates for full-core pin-by-pin depletion problems in Serpent 2 can take up to a few TB of RAM memory [14]. This creates a bottleneck that needs to be tackled in order to be able to run such cases, since the memory available in each single node for any HPC architecture is not sufficient.

In this work, the newly implemented CDD scheme in Serpent 2 [6] is used to address this issue. The method is based on defining domains with only a subset of the burnable materials and associated data, while replicating all other model information, such as geometry, non-burnable materials and spatial tallies, in all

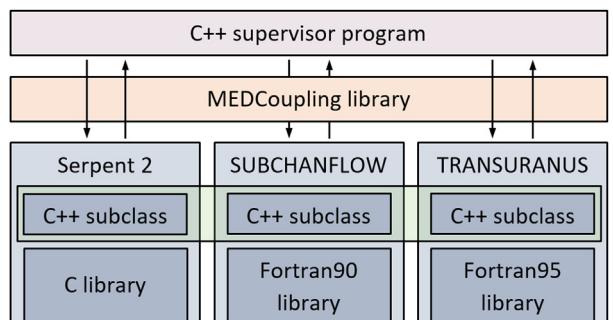


Fig. 1. Software design [5].

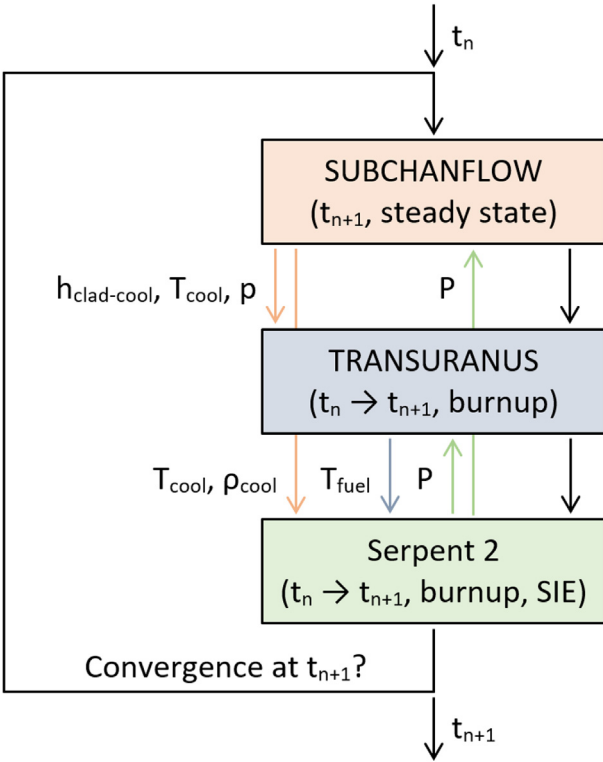


Fig. 2. Depletion scheme [5].

domains. In this way, a problem that does not fit in a single node can be solved adding computing nodes and splitting the memory footprint of the burnup calculation across MPI tasks, each of which associated to a particular domain. The modified tracking algorithm accounts for neutrons flying across domains when they have collisions in non-local materials, but no numerical or physical approximations are made, and therefore the results are equivalent to the traditional domain-replication approach, within their statistical uncertainty. The material decomposition used for the validation case is shown in Section 4.1.

3. Temelín II VVER-1000 validation data

The reactor considered in this work is the Temelín II VVER-1000 NPP [15], with the core characteristics provided in Section 3.1, where proprietary data is excluded. Section 3.2 presents the operational data for the ninth cycle, while the experimental data is described in Section 3.3. The complete specifications of the core and the operating history, as well as the measurements, were provided by ČEZ, the utility which operates the reactor, in the framework of the McSAFE project.

3.1. Core description

The reactor core consists of 163 TVSA-T [16] fuel assemblies of 8 different types organized as shown in Fig. 3, with a fuel-assembly pitch of 23.6 cm. The fuel material is UO₂ with an enrichment between 1.3% and 4% and Gd₂O₃ as burnable poison. The main core parameters at nominal operating conditions are shown in Table 1. The total bypass flow includes all the flow that goes through the guide tubes plus the flow between the core baffle and the barrel.

Each fuel assembly is composed of an hexagonal arrangement of 312 fuel rods, 18 guide tubes and a central instrumentation tube, with the layouts shown in Fig. 4 for each fuel type. Fig. 4 also shows

the fuel enrichment in weight fraction of ²³⁵U and the Gd content in weight fraction of Gd₂O₃. All fuel types have 15 cm of top and bottom axial blankets of natural uranium, except for type a13A, which has a 1.3% enrichment in the whole active length. The pin pitch is 1.275 cm and the active length 368 cm. Fuel assemblies have 8 spacer grids: 7 within the active length and one at the top. The structural components include corner stiffeners welded to the spacer grids, a lower support node to fix the fuel pins and top and bottom nozzles. The cladding and spacer grid material is E110 zirconium alloy, while the guide tubes and stiffeners are made of E635 alloy.

The control rods have B₄C and Dy₂TiO₅ as absorber materials and an absorber length of 354.5 cm, with 324.5 cm of B₄C and 30 cm of Dy₂TiO₅. The cladding is made of 42XHM alloy. There are 61 control rods in total, organized in banks 1 to 10 as shown in Fig. 5. Banks 7 to 10 are used for power regulation, and the rest are used only for shutdown. During regulation close to full power only bank 10 is active, so the model considered in this work includes only this bank.

3.2. Operational data

Fig. 6 shows the thermal power, critical boron concentration, control bank position, inlet temperature and mass flow rate for the ninth burnup cycle of the NPP, which corresponds to the startup cycle with TVSA-T fuel, with the whole core loaded with fresh fuel. Given that the power is close to the nominal value for most of the cycle, an effective full-power operational history with condensed data was considered, in particular for control rods. The calculated critical boron concentration, flux profiles and power distributions were compared with the experimental measurements at the time points marked in Fig. 6 (5–43), where the power has been stable long enough that the xenon can be considered at equilibrium at full power. The control bank position is taken as constant between time points, where the insertion is calculated as an average of the raw data over time weighted with the thermal power. The inlet temperature T_{inlet} and mass flow rate \dot{m} were taken as constant during the whole cycle.

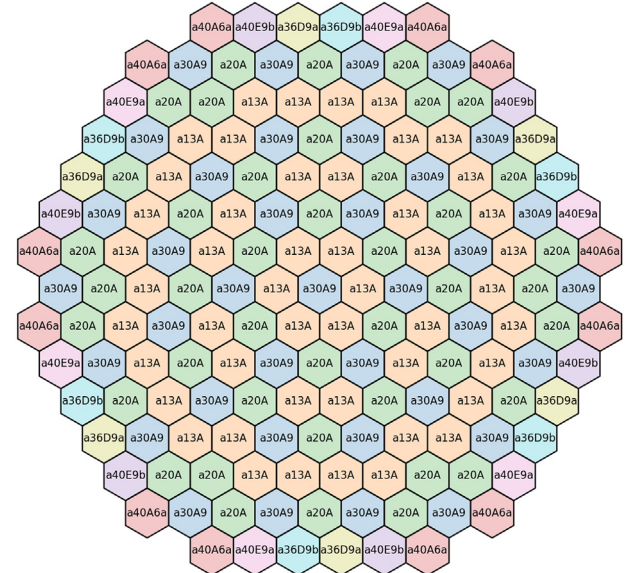


Fig. 3. Core layout. The fuel types are shown in Fig. 4.

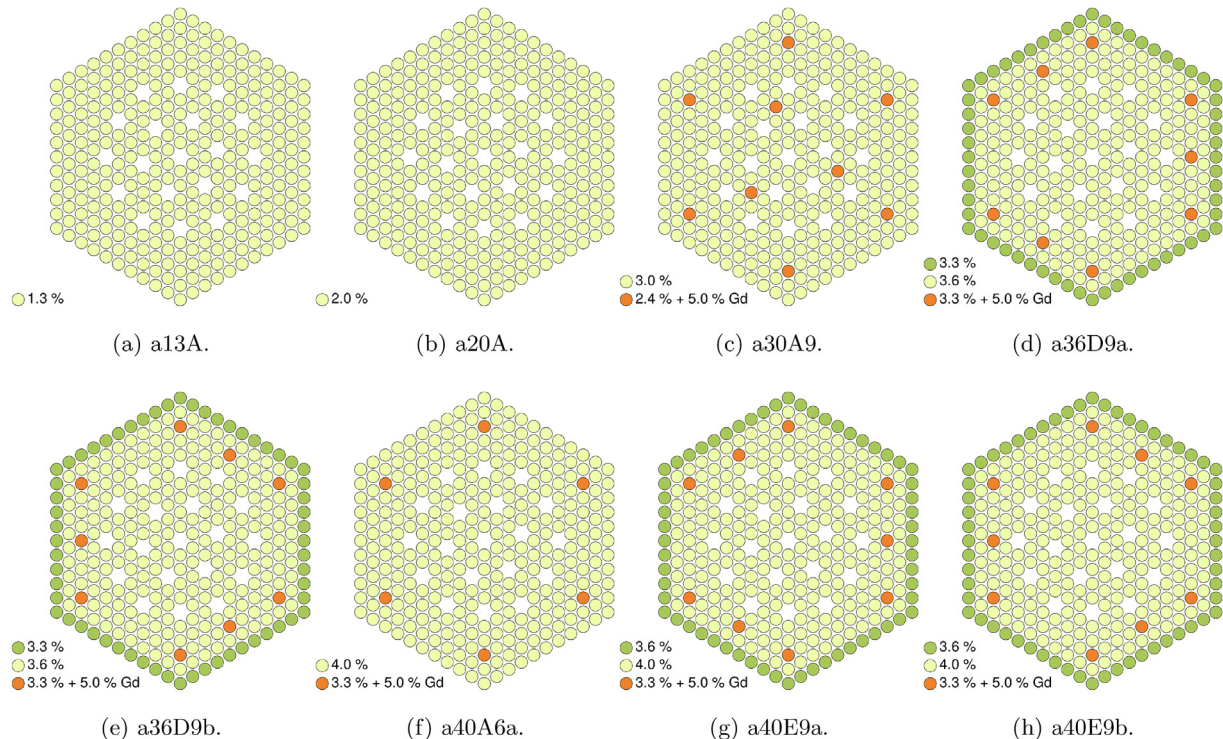


Fig. 4. Fuel-assembly layout for each fuel type. The empty positions correspond to the guide tubes and the central instrumentation tube.

Table 1
Main core parameters.

Parameter	Value
Thermal power	3000 MW
Outlet pressure	15.7 MPa
Total mass flow rate	17909 kg/s
Inlet temperature	288.9 °C
Total bypass flow	3.4%

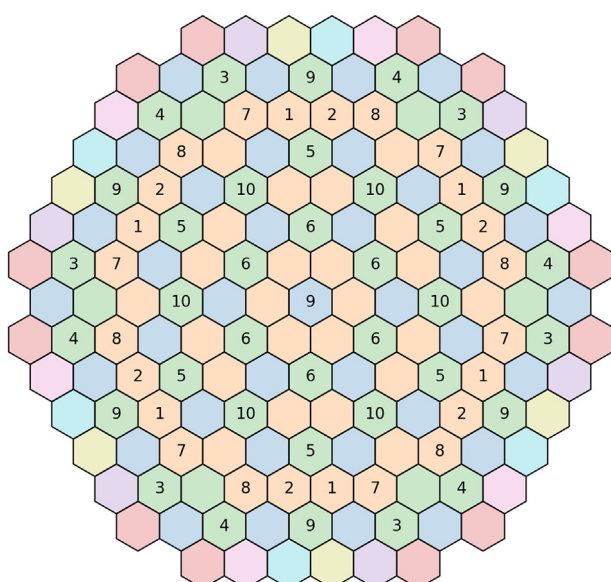


Fig. 5. Control-bank layout.

3.3. Experimental data used for validation

Two sets of experimental data are used in this work to evaluate the accuracy of the numerical calculations: critical boron concentration and direct pin-level neutron flux measurements. The critical boron comes from boric acid (H_3BO_3) concentration measurements during reactor operation and the flux profiles correspond to ^{103}Rh Self Powered Neutron Detector (SPND) [17] readings. The SPNDs are inserted in the central instrumentation tubes (see Fig. 4), with the radial distribution shown in Fig. 7, where the indexing is defined. Axially, each detector consists of a string of 7 SPNDs separated by about 50 cm, with the lowest position approximately 30 cm above the bottom of the fuel stack.

In addition to direct measurements, the axial and radial power profiles reported by the CMS are available to assess the power distribution predicted by Serpent. The CMS reconstructs the power based on the adjustment of a theoretical solution to the SPND data.

All the measured data is available at 43 time points through the operating cycle. The points selected for comparison are the ones shown in Fig. 6.

4. Modeling approach

The burnup calculation was performed at nominal operating conditions, i.e. at full power, with the parameters summarized in Table 1. The burnup steps are the ones marked in Fig. 6 (5–43), for which constant control bank positions were obtained. The calculated neutron flux and power distribution were compared with the experimental data at time points 5 and 43. The convergence tolerance ϵ for the multiphysics iterations at each burnup step (see Fig. 2) are 1%, 1 kg/m^3 and 10 K for the fission power, coolant density and fuel temperature, respectively. The solution is considered converged when

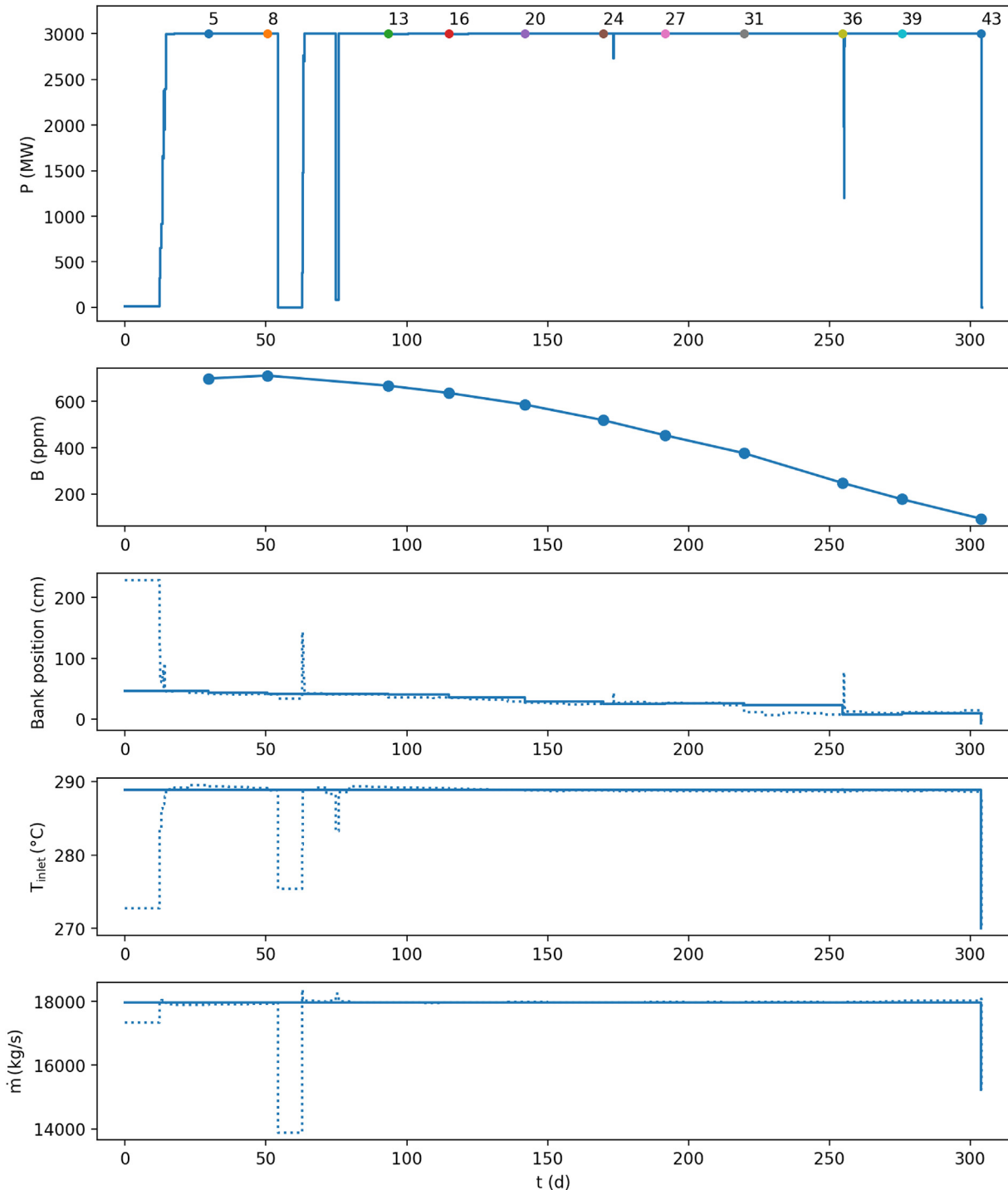


Fig. 6. Thermal power P and measured time points, critical boron concentration B , condensed control bank positions, inlet temperature T_{inlet} and mass flow rate \dot{m} (the raw operational data is shown in dashed line).

$$\|x_i(\vec{r}) - x_{i-1}(\vec{r})\|_{L_2} < \varepsilon, \quad (1)$$

taking the L_2 norm of the difference between the solution $x(\vec{r})$ between the last two iterations i and $i-1$. These criteria are consistent with the stochastic variability of the results, and the solution converged typically after 3 or 4 iterations. Finally, no variance reduction techniques were used, and the source

convergence was checked based on its Shannon entropy. The Serpent, SCF and TU models are summarized in sections 4.1, 4.2 and 4.3 respectively.

4.1. Serpent model

Figs. 8 and 9 show the full-core pin-by-pin Serpent model for xy- and yz-cuts. The core baffle, barrel and spacer grids, as well as axial and radial reflectors, are included in the geometrical model,

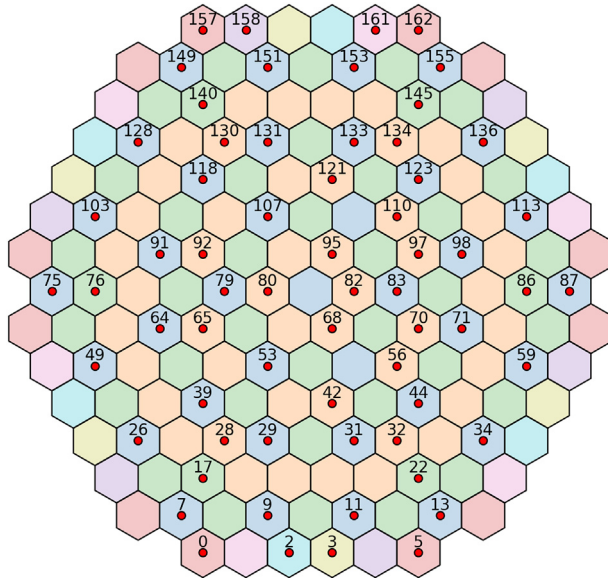


Fig. 7. Radial distribution of SPND strings.

and vacuum boundary conditions are used. A close-up view of the central fuel assembly is shown in Fig. 10. The SPNDs are modeled in Serpent as spatial detectors tallying total neutron absorption in ^{103}Rh , which is the indicator material, assuming that the SPND response is proportional to this quantity.

Each transport calculation was performed using 250 active cycles of 10^6 particles, with the criticality source calculated initially with 100 inactive cycles and corrected with 25 cycles before each iteration. The critical boron concentration was calculated forcing criticality during the inactive cycles, and equilibrium xenon was imposed. The nuclear data corresponds to the JEFF-3.1.1 library [18].

A pin-by-pin material division was used for the burnup calculation, with each pin divided in 16 axial zones. Pins with burnable absorber were further subdivided in 12 radial zones. The total number of burnable materials is 909,330. Figs. 11 and 12 show the

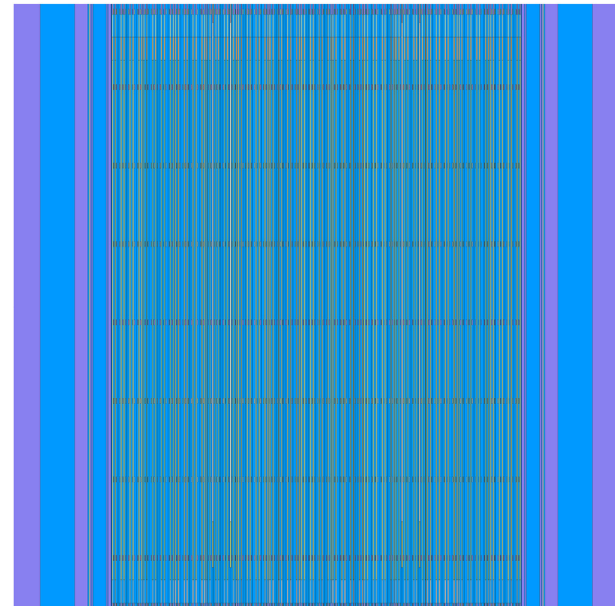


Fig. 9. Serpent model for the whole core (yz-cut).

material-based domain decomposition using 64 domains for cuts along the z and x axis respectively. Each color represents the burnable materials in a given CDD domain, while all the non-burnable materials, such as the moderator and the structures, are replicated. The logic to determine the domain shapes is to use compact regions to minimize the number of particle transfers across domains [6]. It is important to note here that the material decomposition is only a computational issue and has no impact on the results of the burnup calculation, since no physical approximations are introduced by the CDD scheme, as noted in Section 2.3.

4.2. SCF model

Fig. 13 shows the SCF geometry for the whole core, while a close-up view of the central fuel assembly is presented in Fig. 14. The

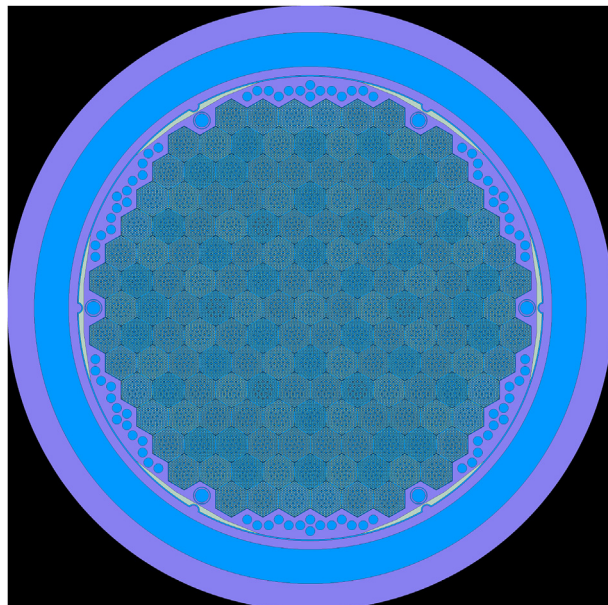


Fig. 8. Serpent model for the whole core (xy-cut).

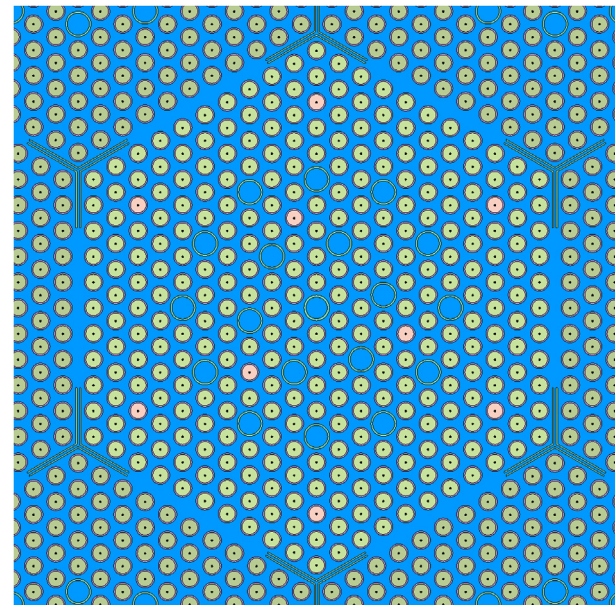


Fig. 10. Serpent model for the central fuel assembly (xy-cut).

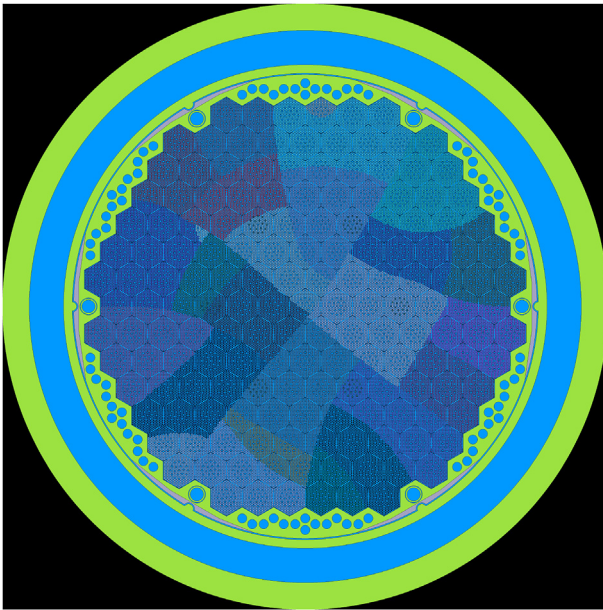


Fig. 11. Serpent material decomposition using 64 domains (xy-cut).

subchannel model is coolant-centered, i.e. the control volumes are defined by the physical channels bounded by the rods, and the power of each rod is divided between the subchannels around it according to the corresponding heated perimeters. The cross-flow model is made up of convective and turbulent contributions, and a constant mixing coefficient that includes the effect of spacer grids is used for the latter. The axial discretization is composed of 30 equidistant nodes for the active length, and localized pressure losses are included in the spacer grid positions. The boundary conditions, i.e. outlet pressure, mass flow-rate and inlet temperature, correspond to Table 1.

When TU is used, the rods are only considered as heat sources to perform the coolant calculation. Otherwise, SCF also solves the fuel temperatures with a simplified fuel-performance model, as

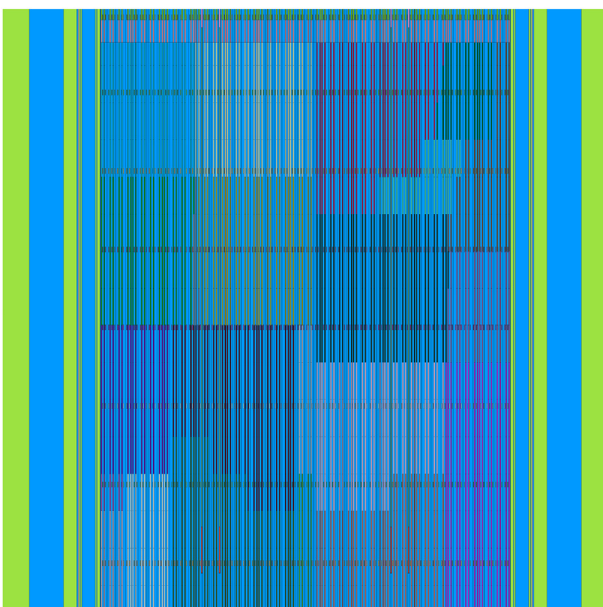


Fig. 12. Serpent material decomposition using 64 domains (yz-cut).

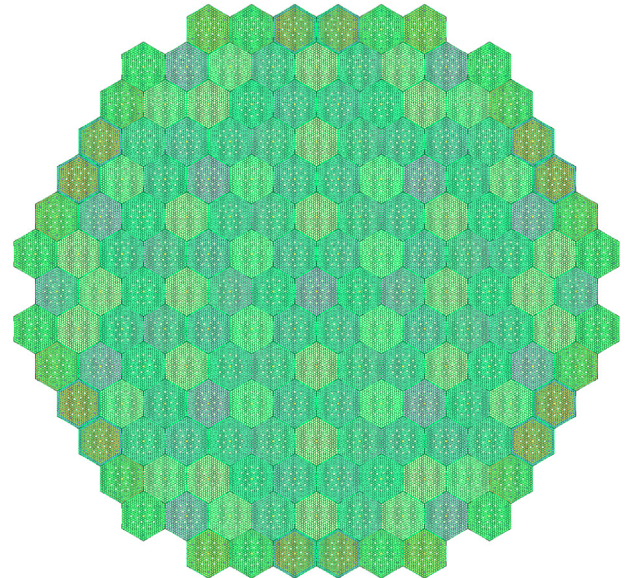


Fig. 13. SCF model for the whole core.

mentioned in Section 2.2, in this case using 10 radial nodes. The fuel-cladding gap width is calculated considering fuel swelling [19] and relocation by cracking [20], as well as pellet and cladding thermal expansion [19]. The gap conductance takes into account heat conduction and thermal radiation through the filling gas, and depends on the gap width and the surface roughnesses. The fuel and cladding heat capacity depend only on temperature [19], while the fuel conductivity correlation also considers burnup [21].

4.3. TU model

The TU model includes all the fuel rods in the system, while guide tubes and instrumentation tubes are not considered. The radial discretization for each rod consists of 6 coarse zones, 4 in the fuel and 2 in the cladding, in which the thermomechanical properties are taken as uniform. The numerical calculation is performed on a fine mesh with 32 radial zones. Axially, each rod is discretized in 30 levels. The coolant temperature and pressure, as well as the cladding-coolant heat transfer coefficient, which are calculated by SCF, are used as boundary conditions on the cladding-coolant interface. While the TU multiphysics module used in this work handles the whole model, the solution of each rod remains independent.

The thermomechanical model takes into account a wide variety of physics, e.g. thermal and irradiation-induced densification of the fuel, swelling due to solid and gaseous fission products, creep, plasticity, pellet cracking and relocation, oxygen and Pu redistribution, volume changes during phase transitions, formation and closure of central void and treatment of axial friction forces.

The fuel-cladding gap conductance is calculated using the URGAP model [22], and depends on the gap width, the gas pressure and composition, and the surface characteristics of the cladding and the fuel. The gap width is a result of the mechanical calculation, which determines the deformation of the pellet and the cladding.

5. Selected results

This section summarizes the results obtained with Serpent-SCF with and without TU, as well as the comparison with the experimental data, for the burnup calculation up to 279.9 EFPD (11.08

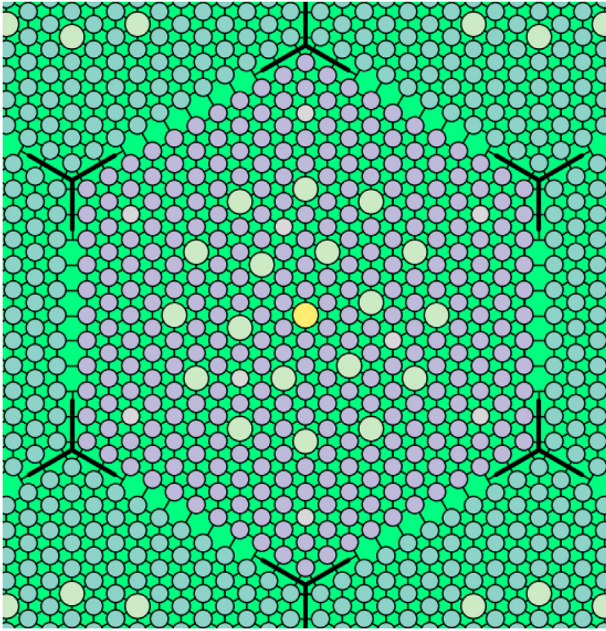


Fig. 14. SCF model for the central fuel assembly.

MWd/kgU). The critical boron concentration, neutron flux profiles and power distribution are presented in sections 5.1 to 5.3, while Section 5.4 introduces additional pin-level results for the whole core.

The simulations were run in the ForHLR II HPC cluster of the Karlsruhe Institute of Technology (KIT) [23] using 64 nodes with 20 cores each (1280 cores in total), with a maximum runtime of 7 days.

5.1. Critical boron concentration

The calculated and measured critical boron concentration is shown in Fig. 15. The Root Mean Square (RMS) difference between the results and the experimental data is 33.8 and 31.5 ppm for Serpent-SCF and Serpent-SCF-TU respectively. The deviations with the measurements are around the acceptability criterion for this type of calculation, which is usually between 50 and 100 ppm, and within the typical uncertainties due to specifications and nuclear data. Moreover, the differences between results with and without TU, which are lower than 7 ppm for the whole range, are not significant. These results serve to verify the calculation of global parameters like reactivity, which involve the burnup simulation with equilibrium xenon and the critical boron iteration.

5.2. Neutron flux profiles

Figs. 16 and 17 show the normalized neutron flux profiles for the two positions with smallest and largest RMS deviations between the Serpent detector responses and the SPND measurements at time points 5 and 43, with the indexing defined in Fig. 7. The error bars correspond to three standard deviations $\sigma(z)$ for each axial location, and the relative differences $\varepsilon(z)$ are calculated as

$$\varepsilon(z) = \frac{\phi(z) - \bar{\phi}_{SPND}(z)}{\bar{\phi}_{SPND}}, \quad (2)$$

where $\phi(z)$ and $\phi_{SPND}(z)$ are the calculated and measured neutron fluxes and $\bar{\phi}_{SPND}$ is the average value for each SPND. Overall, the results are in good agreement with the experimental data, though

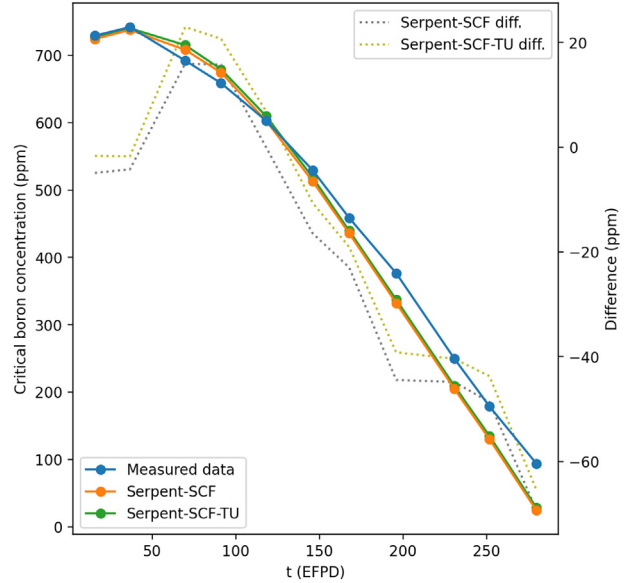


Fig. 15. Calculated and measured critical boron concentration.

significant differences can be observed in the top and bottom positions. The differences between the calculations with and without TU seem to be purely statistical fluctuations, which is in accordance with previous studies [9].

The experimental error is not available and is difficult to estimate, and therefore the measurements are reported without error bars. Moreover, it is hard to assess the accuracy of the solution at the top position of the SPND stack without a proper quantification of the uncertainty in the axial positions of the detectors.

It is important to note here that the reported standard deviations for the results correspond only to the statistical uncertainty in the transport calculation, and do not take into account other factors such as the burnup and thermalhydraulic calculations, which propagate stochastic errors between iterations. The total statistical uncertainty is actually higher, and in principle can only be obtained running the calculation multiple times to calculate the real deviations, which is not possible in this case due to the large runtimes involved.

Fig. 18 shows the normalized radial distribution of the neutron flux SPND measurements at time points 5 and 43, while Figs. 19 and 20 present the results and their deviations with respect to the experimental data. The relative differences $\varepsilon(r)$ are calculated as

$$\varepsilon(r) = \frac{\phi(r) - \bar{\phi}_{SPND}(r)}{\bar{\phi}_{SPND}}, \quad (3)$$

where $\phi(r)$ and $\phi_{SPND}(r)$ are the calculated and measured neutron fluxes axially averaged at each radial position and $\bar{\phi}_{SPND}$ is the average value for the whole core.

Fig. 21 shows the total RMS deviations between the results and the SPND measurements for the whole burnup calculation. These are calculated as an RMS average of the local deviation $\varepsilon(z)$ over all SPND positions for each time point. The differences tend to decrease slightly with burnup, and the average is 11.2% and 11.3% for Serpent-SCF and Serpent-SCF-TU respectively.

5.3. Power distribution

Fig. 22 shows the results and CMS reconstruction for the axial power profile at time points 5 and 43. The calculated profiles are in

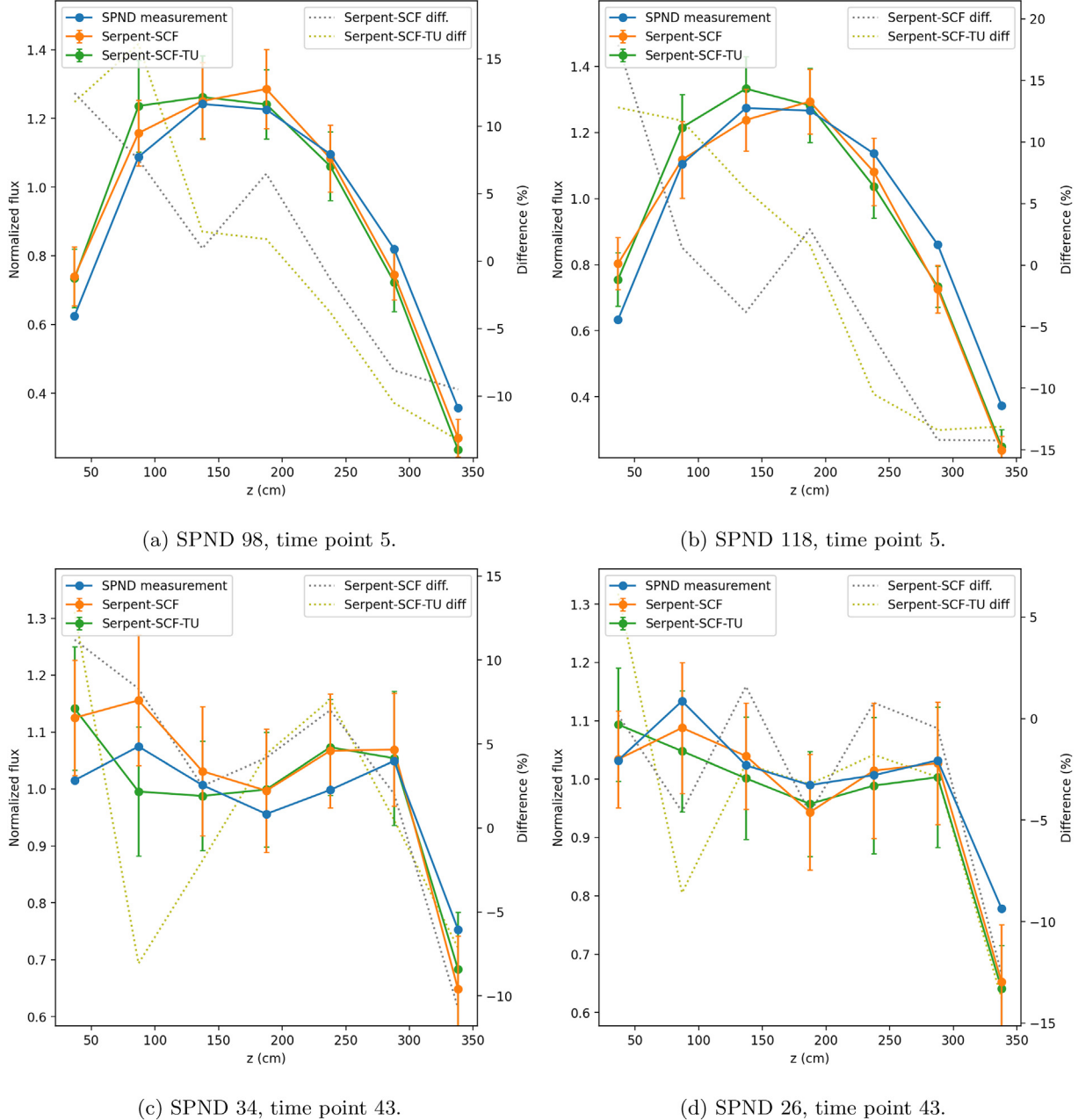


Fig. 16. Calculated and measured neutron flux for the SPNDs with the smallest RMS deviations (the active length starts at $z = 0$).

very good agreement, and the differences are concentrated in spacer grid positions, where the Serpent calculation is expected to be more accurate than the CMS solution.

The radial power distribution reported by the CMS at time points 5 and 43 is shown in Fig. 23, while Figs. 24 and 25 present the results and their deviations with respect to the CMS. The statistical error for the results corresponds to three standard deviations $\sigma(r)$ and the relative differences $\varepsilon(r)$ are calculated as

$$\varepsilon(r) = \frac{P(r) - P_{CMS}(r)}{\bar{P}_{CMS}}, \quad (4)$$

where $P(r)$ and $P_{CMS}(r)$ are the calculated and reported power distributions and \bar{P}_{CMS} is the average power for the whole core. The differences between the results and the CMS are consistent with

the deviations found in the SPND measurements, shown in Figs. 19 and 20.

5.4. Pin-level results

As shown in the previous sections, the impact of including fuel-performance capabilities in the calculation system does not influence the neutronic results in a significant way, at least not for the burnup calculations considered here. This is in line with previous investigations dealing with smaller-scale problems [9]. However, the main advantage of the three-code approach used in this work is the ability to simulate the neutronic, thermalhydraulic and thermomechanical behavior of the core with a fully coupled high-fidelity scheme. In particular, the fuel-performance calculation is done within the burnup simulation, obtaining a fuel solution with full

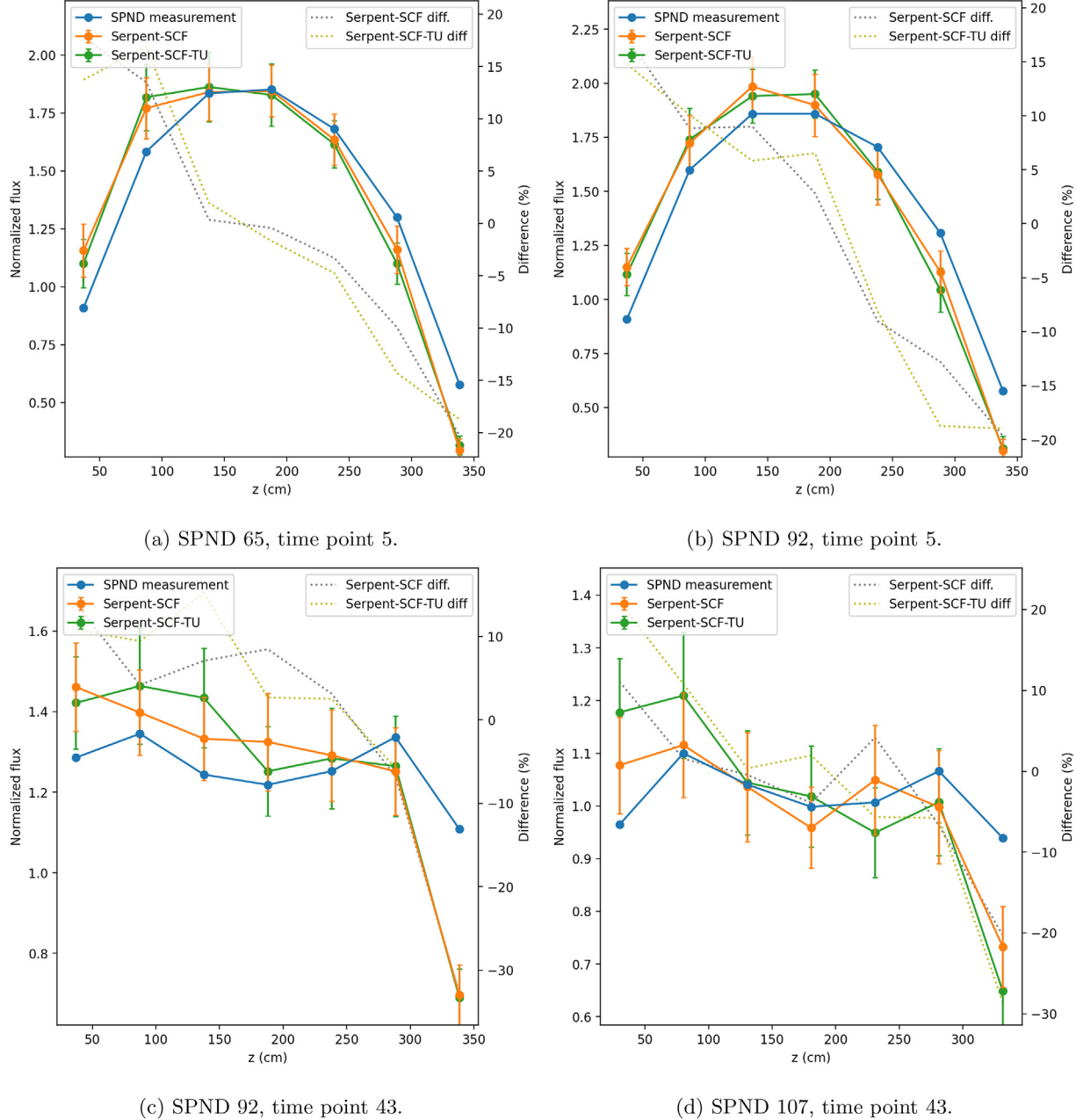


Fig. 17. Calculated and measured neutron flux for the SPNDs with the largest RMS deviations (the active length starts at $z = 0$).

detail for consistent core states.

Fig. 26 shows the power calculated by Serpent at End of Cycle (EOC), as well as the coolant temperature solved by SCF. This level of detail allows for the direct calculation of local safety parameters at pin level, as well as a realistic description of the core to perform the pin-by-pin burnup calculation and the fuel-performance analysis.

Fig. 27 presents the fuel-cladding gap solution predicted by TU at EOC. While the gap behavior does not necessarily play an important role in the burnup calculation presented here, it is a relevant parameter in transient simulations and safety analysis. Obtaining the gap size and conductance from TU, which has been extensively validated for PWR and VVER designs [4,24], is a key benefit of this approach.

Finally, the fuel centerline temperature and the Xe fission-gas

release calculated by TU at EOC are shown in Fig. 28. These safety-relevant parameters are obtained from TU as a result of the thermomechanical calculation.

6. Discussion

This section presents a summary of the validation results, as well as a discussion on the calculation methodologies used in this work.

6.1. Validation summary

Overall, the results obtained with Serpent-SCF with and without TU are in quite good agreement with the experimental data. The deviations between the calculated and measured critical boron

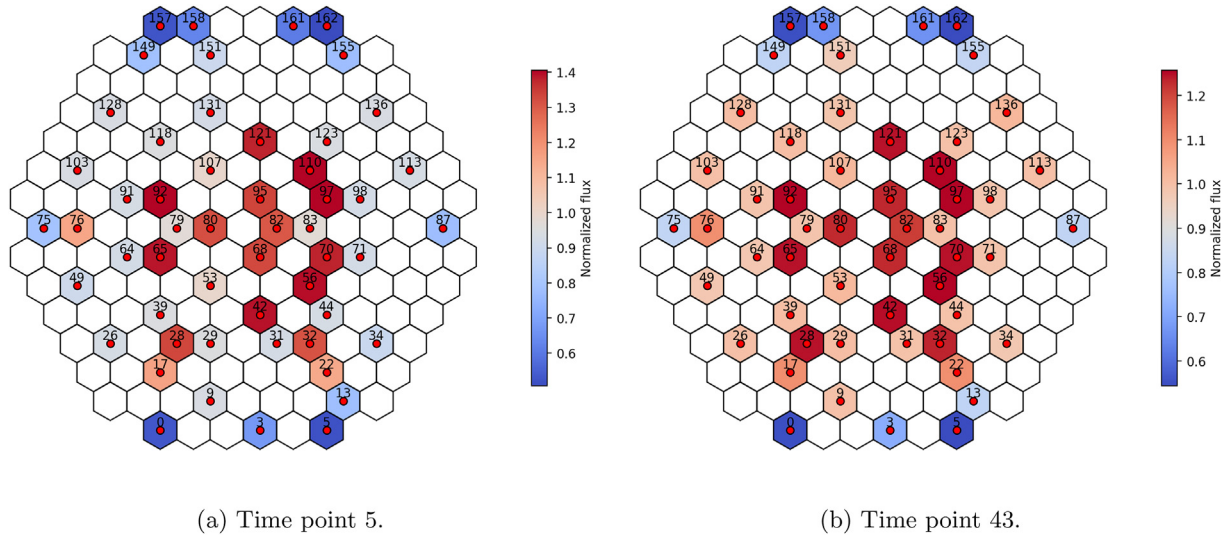


Fig. 18. Radial (axially averaged) neutron flux SPND measurements.

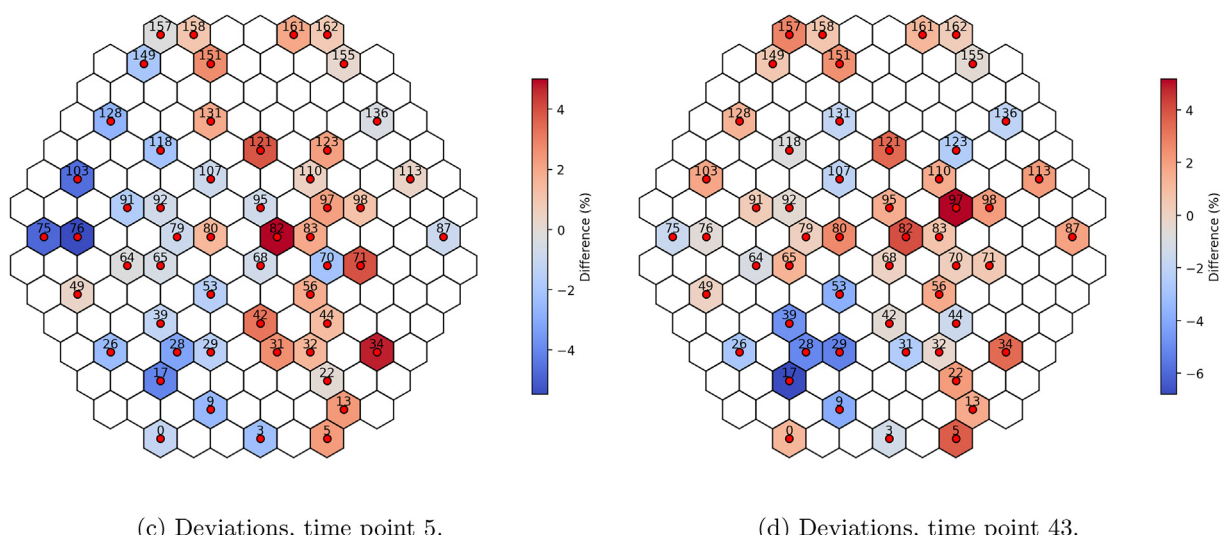
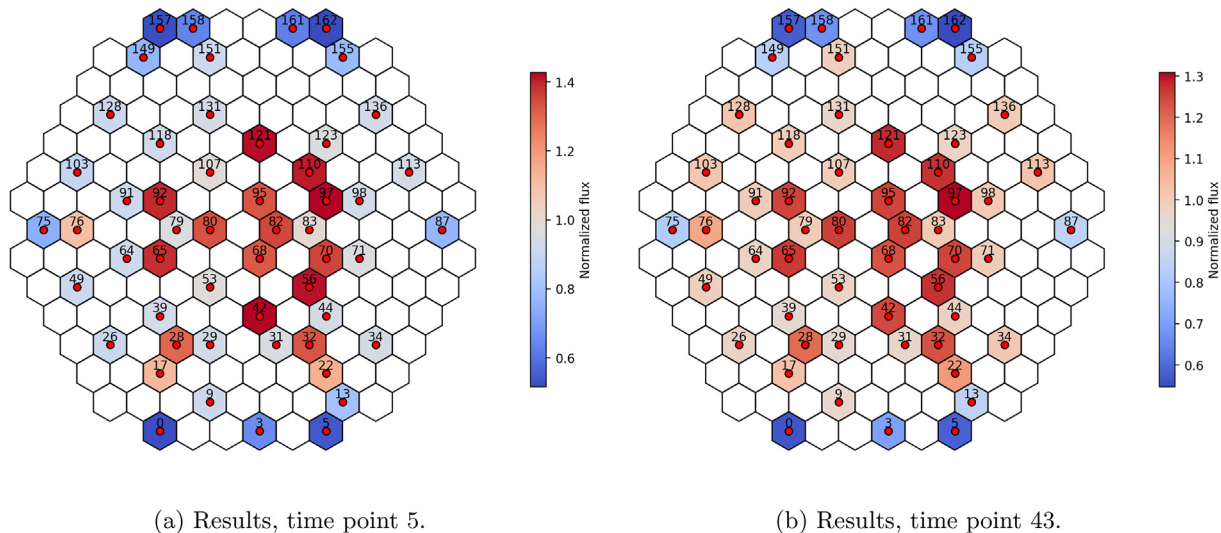


Fig. 19. Radial (axially averaged) neutron flux Serpent-SCF results and deviations against the SPND measurements.

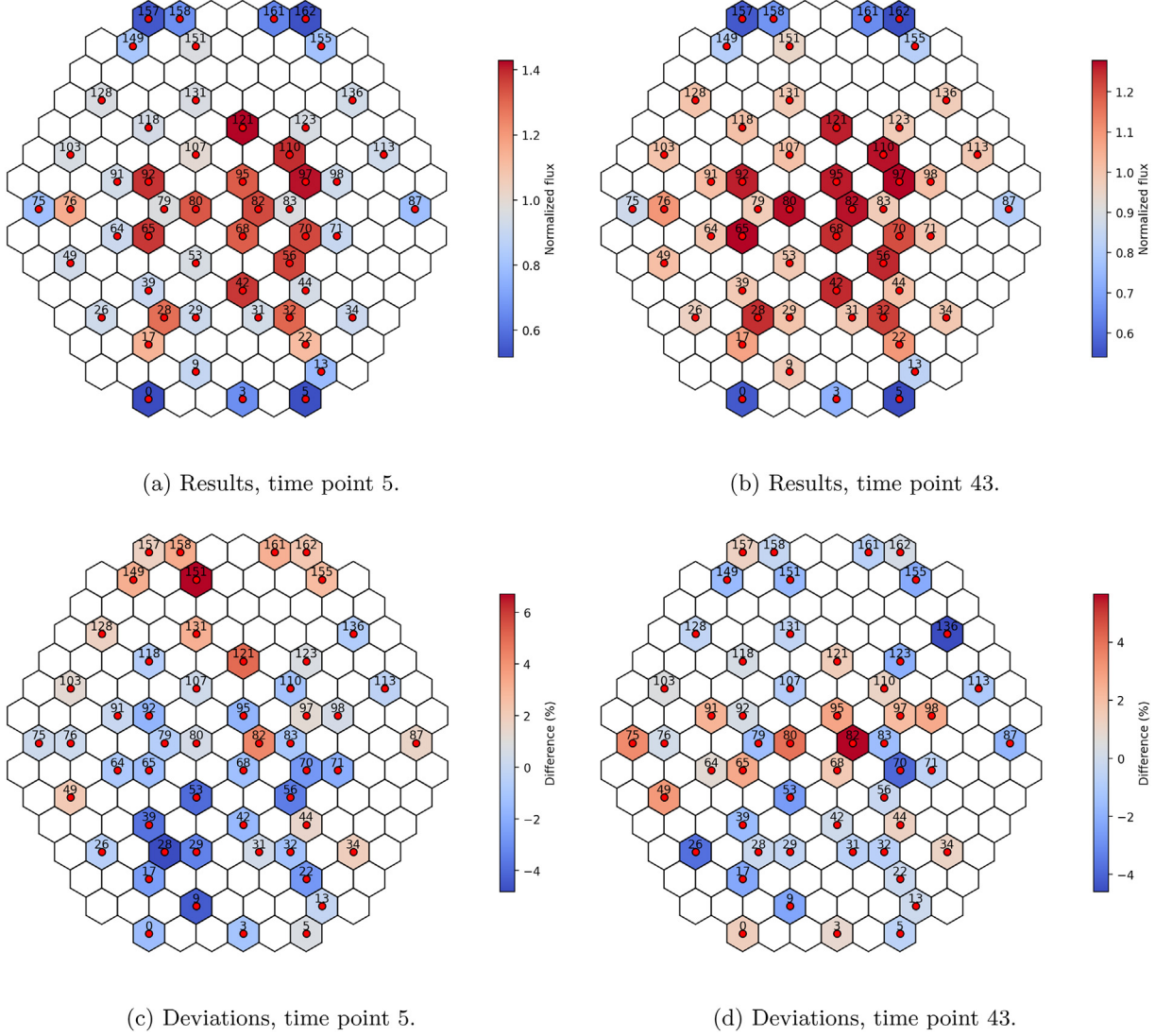


Fig. 20. Radial (axially averaged) neutron flux Serpent–SCF–TU results and deviations against the SPND measurements.

concentrations are below 70 ppm for the whole cycle, which is within the typical acceptability criterion for these kind of calculations. The pin-level neutron flux profiles obtained with Serpent are consistent with the SPND measurements within their statistical uncertainty in most cases, with the exception of larger differences (up to 30%) at the core top section. The calculated axial and radial power profiles are in very good agreement with the core monitoring system, with mean differences below 3%. These results demonstrate the accuracy of the simulation tool, both in terms of global behavior and of local pin-level parameters.

6.2. Neutronic feedback to TU

While the coupling scheme used in this work captures the main interaction mechanisms in the system, the neutronic feedback to TU could in principle be refined. On the one hand, radial power profiles could be tallied by Serpent and used directly in the thermomechanical simulation instead of calculating them in TU from the total pin power. However, doing this would dramatically increase the number of particles needed to obtain statistically meaningful values for the radial power profiles for each rod and axial level, which is not feasible in full-core pin-by-pin calculations. On the other hand, the burnup calculation could be performed only in Serpent and the isotope concentrations transferred to TU. The

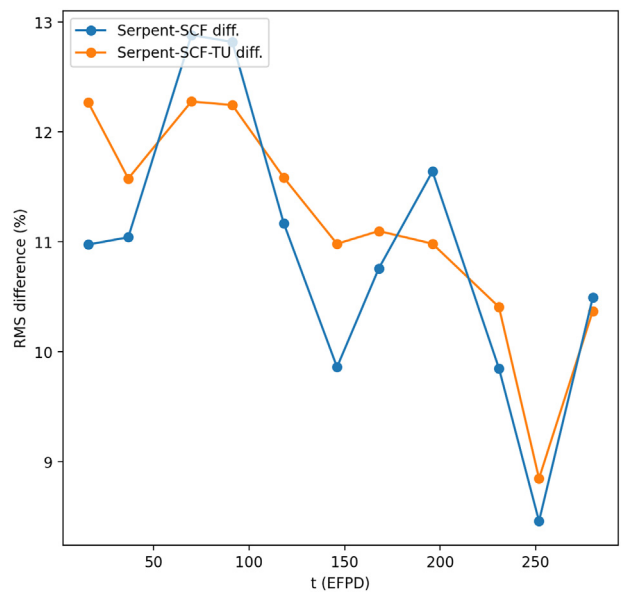


Fig. 21. Total RMS deviations between the neutron flux results and the SPND measurements as a function of burnup.

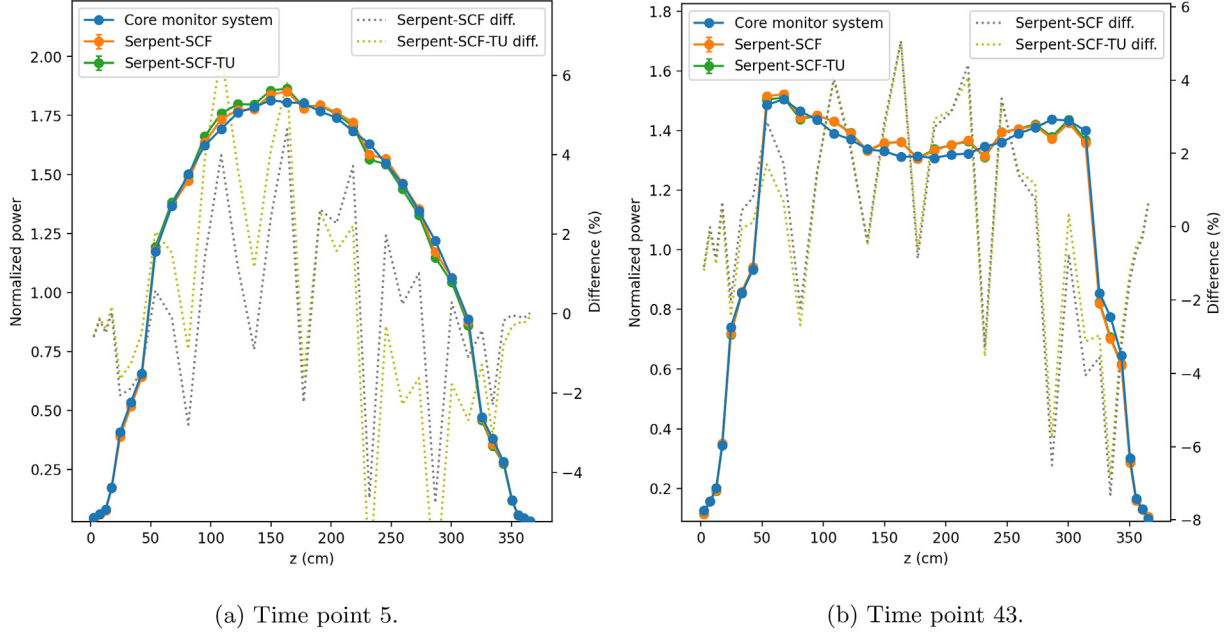


Fig. 22. Results and CMS reconstruction for the axial power profile.

drawback of this approach is that it involves massive amounts of feedback data, considering the radial dependence of material compositions. Moreover, the multiphysics interface in Serpent, which is extremely convenient to exchange power, density and temperature distributions, is not suitable for obtaining material data. For this reasons, the internal TU neutronic model is used in the current implementation, although this issue merits further investigation.

6.3. Impact of including fuel-performance analysis

The results presented in this work show that using a fuel-performance code to improve the fuel modeling does not seem to have a significant impact on the neutronic solution during burnup, for which a standard subchannel code like SCF is quite adequate.

This might not be true for transient calculations where fuel parameters such as gap width and conductance play a major role.

6.4. Additional remarks on the calculation method

The calculation system used in this work provides significant capabilities for high-fidelity core analysis. On the one hand, the ability to handle full-core pin-by-pin burnup problems in Serpent, which is enabled by the newly implemented CDD scheme, is a key feature. In this way, depletion calculations can be performed directly using continuous-energy nuclear data and an extremely detailed geometrical representation, which provides a high-fidelity alternative to the traditional multistep approach based on lattice- and core-level computations. On the other hand, the three-code coupling combining Monte Carlo neutron transport, subchannel

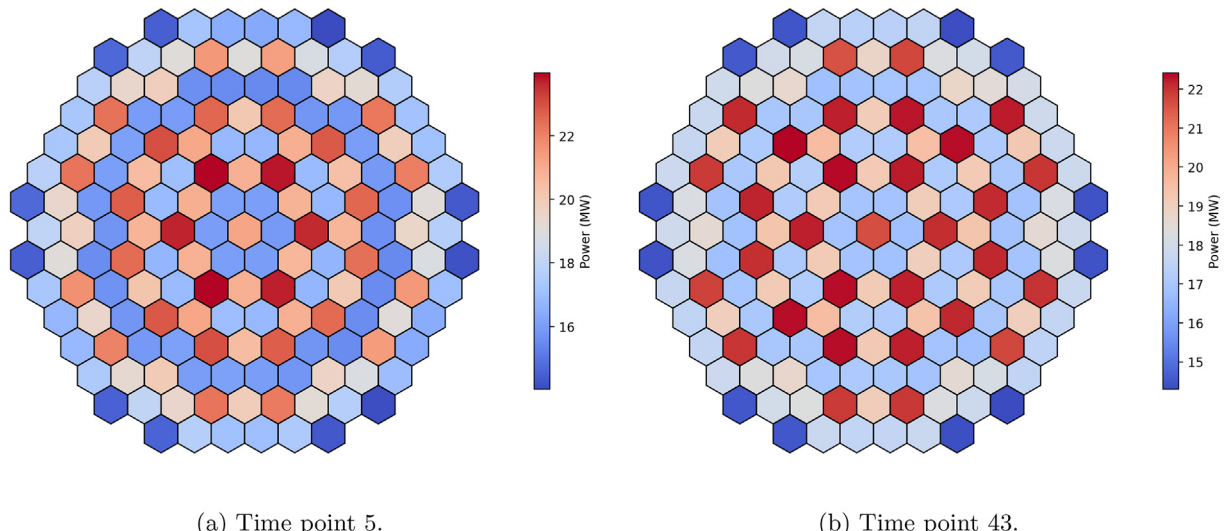


Fig. 23. CMS reconstruction for the radial power distribution.

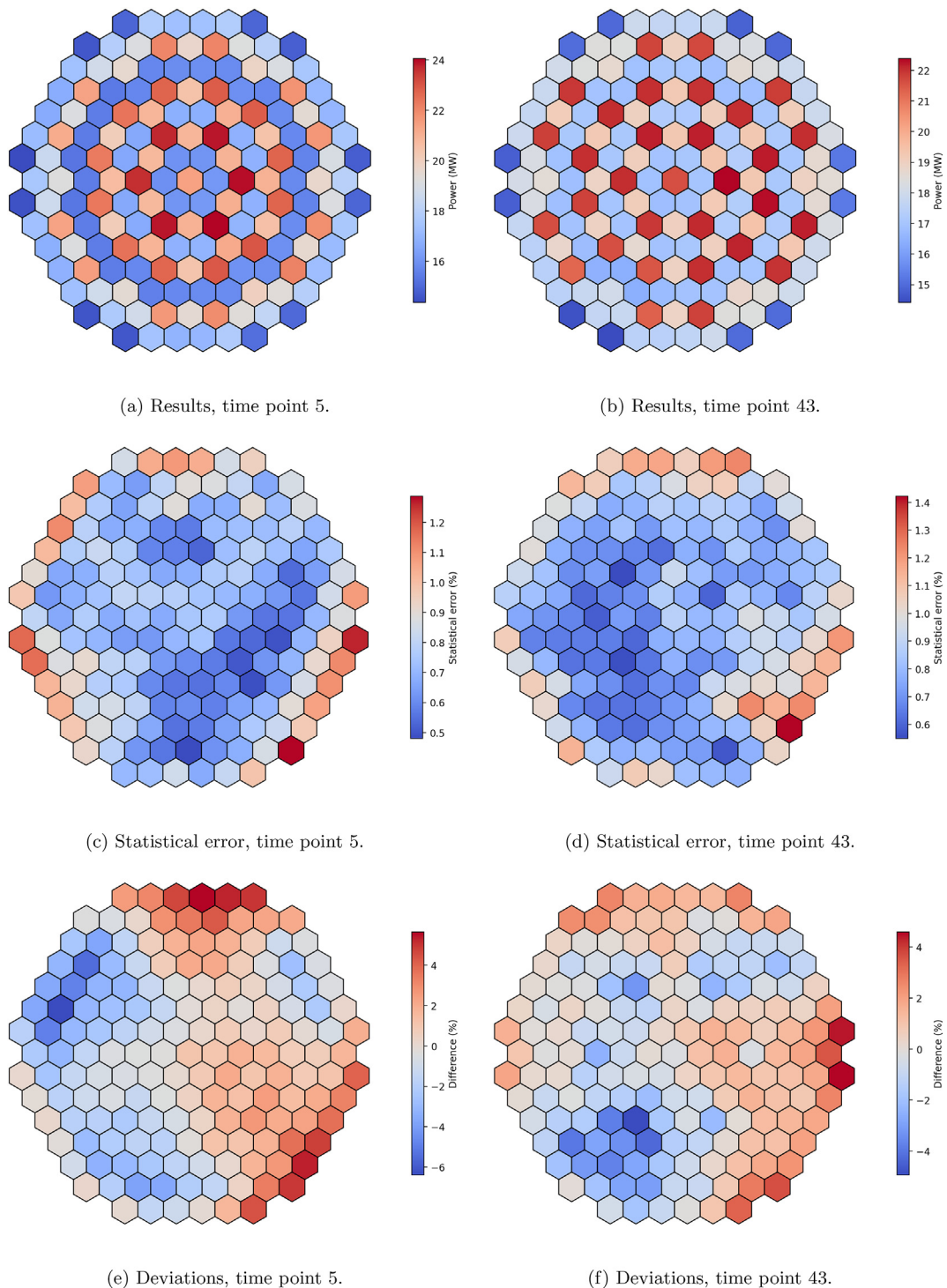


Fig. 24. Serpent-SCF results and statistical error (3σ) for the radial power distribution and deviations against the CMS.

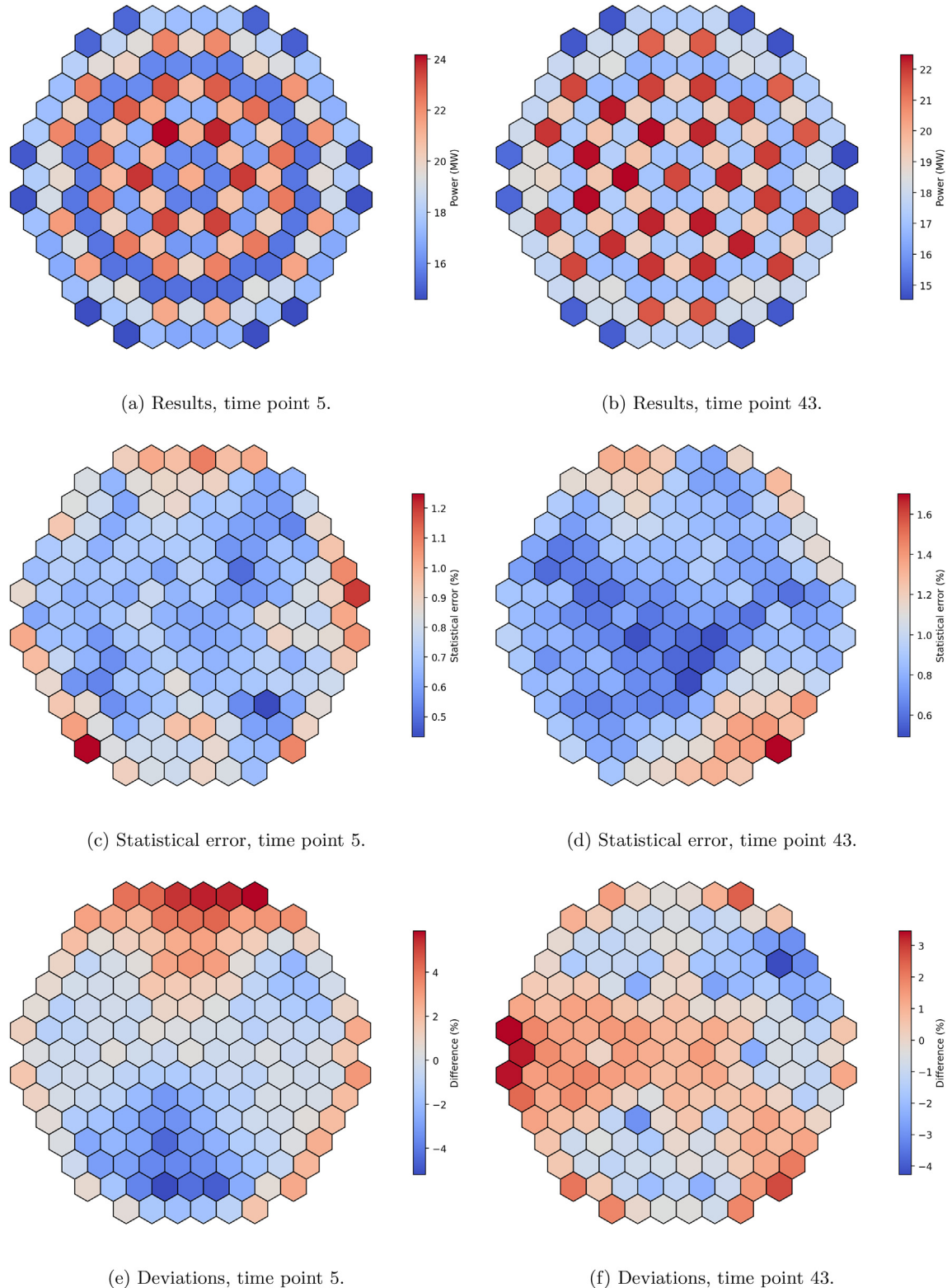


Fig. 25. Serpent–SCF–TU results and statistical error (3σ) for the radial power distribution and deviations against the CMS.

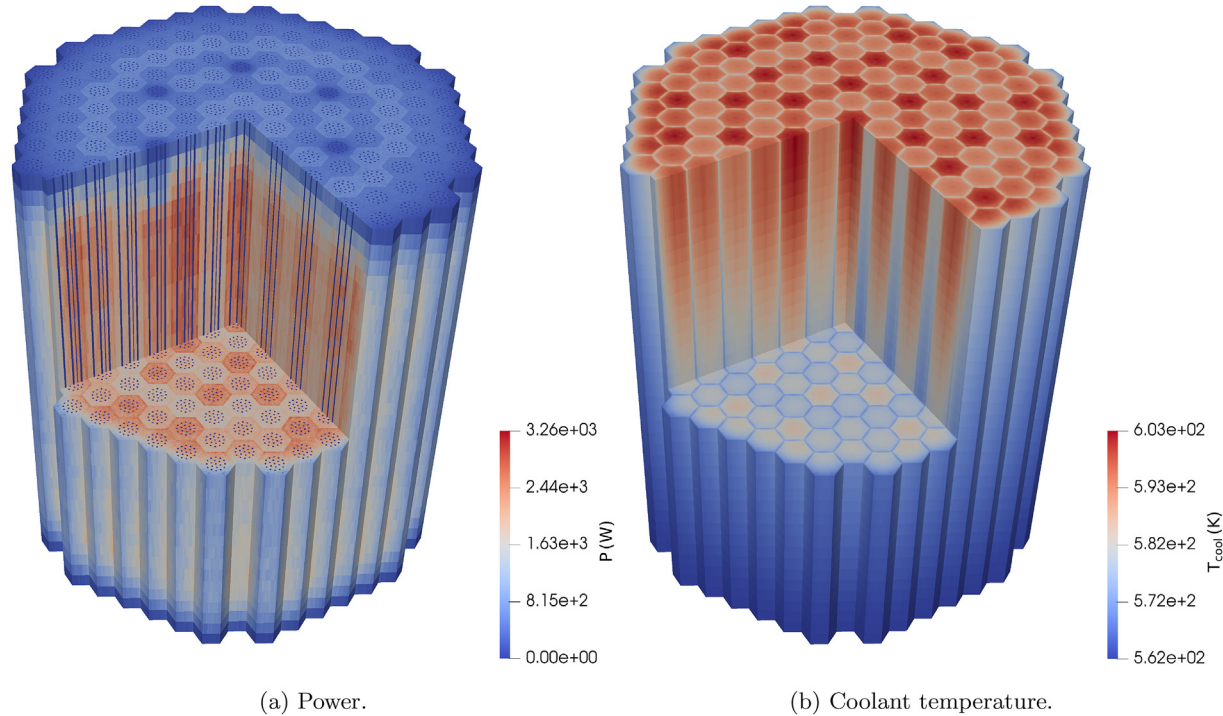


Fig. 26. Serpent power and SCF coolant temperature at time point 43 (11.08 MWd/kgU).

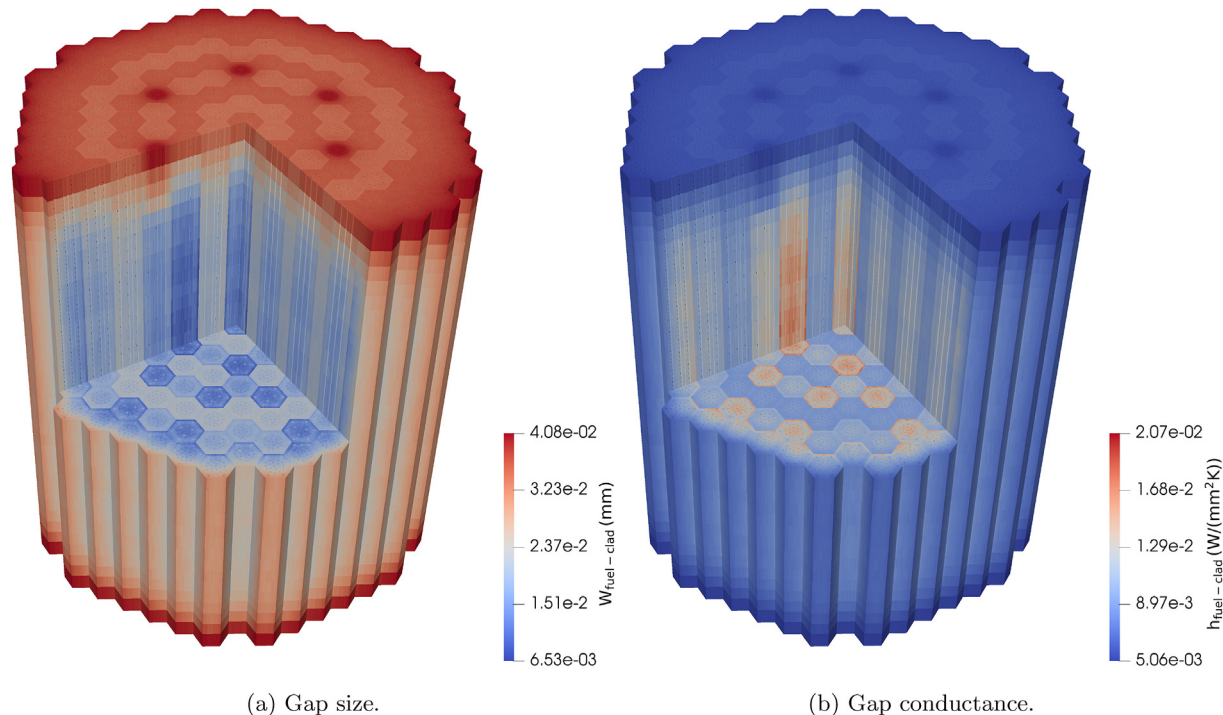


Fig. 27. Fuel-cladding gap solution at time point 43 (11.08 MWd/kgU).

thermalhydraulics and fuel-performance analysis provides a very valuable framework to perform a thorough analysis of the core for realistic conditions. Even if the impact of the thermomechanic solution on the neutronics is not significant, a complete fuel-performance analysis of the core is carried out as part of the burnup calculation. As a result, most parameters of interest for both design and safety analysis can be obtained directly from a single simulation.

7. Conclusions

In the framework of the EU Horizon 2020 McSAFE project, a Serpent–SCF–TU coupling was developed and tested, along with a domain decomposition scheme to handle massive depletion problems in Serpent 2. The aim of this simulation tool is to perform full-core pin-by-pin burnup calculations for LWR cores using a fully

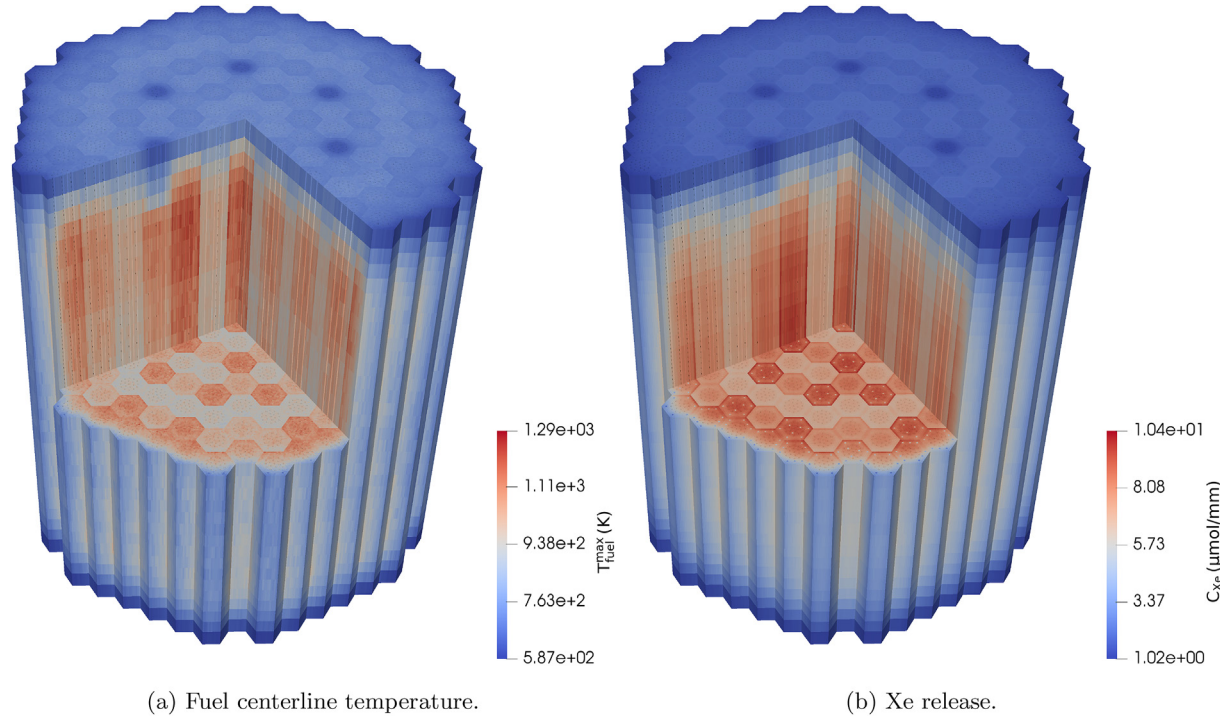


Fig. 28. Fuel solution at time point 43 (11.08 MWd/kgU).

coupled neutronic-thermalhydraulic-thermomechanic approach. This high-fidelity methodology allows for the direct calculation of burnup-dependent design and safety parameters.

This work presents the validation of this three-code system using measured critical boron concentration and neutron flux profiles, as well as axial and radial power distributions reconstructed by the core monitoring system, for the ninth operating cycle of the Temelín II VVER-1000 power plant. The results are in very good agreement with the experimental data, for simulations with Serpent-SCF with and without TU. While no significant differences in the neutronic solution are found when using TU, the full thermomechanical analysis provides a thorough and consistent description of the reactor core during irradiation. The high-fidelity capabilities of the three-code coupling system are demonstrated with pin-level results for neutronic, thermalhydraulic and thermomechanic fields, in particular for safety-relevant parameters.

Declaration of competing interest

The authors declare that they have no known competing financial interests or personal relationships that could have appeared to influence the work reported in this paper.

Acknowledgments

This work was done within the McSAFE project which is receiving funding from the Euratom research and training programme 2014–2018 under grant agreement No 755097.

This work was performed on the computational resource ForHLR II funded by the Ministry of Science, Research and the Arts Baden-Württemberg and DFG ("Deutsche Forschungsgemeinschaft").

References

- [1] V. Sanchez-Espinoza, L. Mercatali, J. Leppänen, R. Vočka, The McSAFE project - high-performance Monte Carlo based methods for safety demonstration: from proof of concept to industry applications, in: PHYSOR 2020 Conference, Cambridge, UK, April, 2020.
- [2] J. Leppänen, M. Pusa, T. Viitanen, V. Valtavirta, T. Kaltiaisenaho, The Serpent Monte Carlo code: status, development and applications in 2013, Ann. Nucl. Energy 82. doi:10.1016/j.anucene.2014.08.024.
- [3] U. Imke, V. Sanchez-Espinoza, Validation of the subchannel code SUBCHANFLOW using the NUPEC PWR tests (PSBT), Science and Technology of Nuclear Installations (2012), <https://doi.org/10.1155/2012/465059>.
- [4] P. Van Uffelen, C. Györi, A. Schubert, J. van de Laar, Z. Hózer, G. Spykman, Extending the application range of a fuel performance code from normal operating to design basis accident conditions, J. Nucl. Mater. 383 (1). doi:10.1016/j.jnucmat.2008.08.043.
- [5] M. García, R. Tuominen, A. Gommlich, D. Ferraro, V. Valtavirta, U. Imke, P. Van Uffelen, L. Mercatali, V. Sanchez-Espinoza, J. Leppänen, S. Klem, A Serpent2-SUBCHANFLOW-TRANSURANUS coupling for pin-by-pin depletion calculations in Light Water Reactors, Ann. Nucl. Energy 139. doi:10.1016/j.anucene.2019.107213.
- [6] M. García, J. Leppänen, V. Sanchez-Espinoza, A Collision-based Domain Decomposition scheme for large-scale depletion with the Serpent 2 Monte Carlo code, Ann. Nucl. Energy 152. doi:10.1016/j.anucene.2020.108026.
- [7] K. Wang, S. Liu, Z. Li, G. Wang, J. Liang, F. Yang, Z. Chen, X. Guo, Y. Qiu, Q. Wu, J. Guo, X. Tang, Analysis of BEAVRS two-cycle benchmark using RMC based on full core detailed model, Prog. Nucl. Energy 98. doi:10.1016/j.pnucene.2017.04.009.
- [8] J. Yu, H. Lee, M. Lemaire, H. Kim, P. Zhang, D. Lee, Fuel performance analysis of BEAVRS benchmark Cycle 1 depletion with MCS/FRAPCON coupled system, Ann. Nucl. Energy 138. doi:10.1016/j.anucene.2019.107192.
- [9] M. García, R. Tuominen, A. Gommlich, D. Ferraro, V. Valtavirta, U. Imke, P. Van Uffelen, L. Mercatali, V. Sanchez-Espinoza, J. Leppänen, S. Klem, Serpent2-SUBCHANFLOW-TRANSURANUS pin-by-pin depletion calculations for a PWR fuel assembly, in: PHYSOR 2020 Conference, Cambridge, UK, April, 2020.
- [10] CEA/DEN, EDF R&D, OPEN Cascade, SALOME platform documentation: MED-Coupling user's guide. <docs.salome-platform.org/7/dev/MEDCoupling/index.html>. (Accessed 11 November 2020).
- [11] J. Dufek, D. Kotlyar, E. Shwageraus, The stochastic implicit Euler method - a stable coupling scheme for Monte Carlo burnup calculations, Ann. Nucl. Energy 60. doi:10.1016/j.anucene.2013.05.015.

- [12] J. Leppänen, A. Isotalo, Burnup calculation methodology in the serpent 2 Monte Carlo code, in: PHYSOR 2012 Conference, Knoxville, USA, April, 2012.
- [13] A. Schubert, P. Van Uffelen, J. van de Laar, C. T. Walker, W. Haeck, Extension of the TRANSURANUS burn-up model, *J. Nucl. Mater.* 376. doi:10.1016/j.jnucmat.2008.01.006.
- [14] D. Ferraro, M. García, L. Mercatali, V. Sanchez-Espinoza, J. Leppänen, V. Valtavirta, Foreseen capabilities, bottlenecks identification and potential limitations of Serpent MC transport code in large-scale full 3-D burnup calculations, in: ICONE26 Conference, London, UK, July, 2018, <https://doi.org/10.1115/ICONE26-82305>.
- [15] ČEZ Group, NPP Temelin, www.cez.cz/en/energy-generation/nuclear-power-plants/temelin. (Accessed 11 November 2020).
- [16] O.B. Samoilov, V.B. Kajdalov, A.A. Falkov, V.A. Bolnov, O.N. Morozkin, V.L. Molchanov, A.V. Ugryumov, TVSA-T fuel assembly for Temelin NPP. Main results of design and safety analyses, in: Trends of Development, VVER-2010: Experience and Perspectives Conference, Prague, Czech Republic, November, 2010.
- [17] G. G. Kim, N. Z. Cho, Investigation of the sensitivity depletion laws for rhodium self-powered neutron detectors (SPNDs), *Nuclear Engineering and Technology* 33.
- [18] OECD/NEA Data Bank, reportThe JEFF-3.1.1 Nuclear Data Library, JEFF Report 22, OECD/NEA Data Bank.
- [19] D. L. Hagrman, G. A. Reymann, reportMATPRO-version 11: a Handbook of Materials Properties for Use in the Analysis of Light Water Reactor Fuel Rod Behavior, NUREG/CR-0497, TREE-1280 Technical Report, Idaho National Laboratory.
- [20] M. E. Cunningham, C. E. Beyer, reportGT2R2: an Updated Version of GAPCONTHERMAL-2, NUREG/CR-3907, PNL-5178 Technical Report, Pacific Northwest National Laboratory.
- [21] K. Geelhood, W. Luscher, P. Raynaud, I. Porter, reportFRAPCON-4.0: A Computer Code for the Calculation of Steady-State, Thermal-Mechanical Behavior of Oxide Fuel Rods for High Burnup, PNNL-19418 Technical Report, Pacific Northwest National Laboratory.
- [22] K. Lassmann, F. Hohlefeld, The revised URGAP model to describe the gap conductance between fuel and cladding, *Nucl. Eng. Des.* 103 (2). doi:10.1016/0029-5493(87)90275-5.
- [23] Steinbuch Centre for Computing (SCC), ForHLR II documentation. www.scc.kit.edu/dienste/forhlr2.php. (Accessed 11 November 2020).
- [24] P. Van Uffelen, A. Schubert, J. Laar, C. Györi, D. Elenkov, S. Boneva, M. Georgieva, S. Georgiev, Z. Hózer, D. Märkens, G. Spykman, C. Hellwig, Á. Nordström, L. Luzzi, V.D. Marcello, L. Ott, The verification of the TRANSURANUS fuel performance code - an overview, in: 7th International Conference on WWER Fuel Performance, Modelling and Experimental Support, Albena, Bulgaria, September, 2007.